



## PROPAGATION OF SHOCK WAVES IN SOLAR WIND FOR DIFFERENT BOUNDARY CONDITIONS

\*SUBODH KUMAR SHARMA AND \*\*SHIVENDU TRIPATHI

\*S.S.V. College Hapur

\*\*Satish Chandra College, Ballia

---

### **ABSTRACT**

*This article examines observations as well as theoretical models, but its primary focus is on the large-scale characteristics of the disturbances in the solar wind that are associated with interplanetary shock waves and the connection between those disruptions and solar activity. Shock waves, as far as we are aware at the present time, travel ahead of plasma and magnetic fields that are created during solar flares along a broad front in the solar wind that is nearly spherical in shape. Around two days after the flare's initial source, the shock front of moderate strength (Mach number = 2) often reaches 1 AU. The generation of both type II and type IV radio bursts by a flare appears to be the strongest indicator of shock production, despite the fact that not all enormous flares result in the detection of detectable interplanetary shock waves. The theoretical models of shock propagation in the solar wind can explain not only the shock strength but also the transit duration and the shape of the shock. According to both observations and theory, the flare releases into the shock wave, on an hourly time scale, a mass of  $5 \times 10^{21}$  gm and an energy of  $1.6 \times 10^{32}$  ergs. This information is based on the assumption that the two quantities are proportional to one another. The shock waves caused by solar flares represent a significant energy loss mechanism, according to this estimation of the amount of energy released.*

**Keywords:** shock strength, solar activity

### **INTRODUCTION**

The existence of interplanetary shock waves was deduced from the quick rising times of geomagnetic abrupt impulses in the era before the age of direct interplanetary measurements. Propagation of shock waves in an ambient interplanetary medium became the focus of quantitative theoretical models not long after their development. Since their first direct observation by the Mariner 2 spacecraft in 1962, interplanetary shock waves have been the focus of much research, both theoretical and observational. The majority of this research has concentrated on the more local and granular elements of the shock front. In contrast, we focus on the connection between interplanetary shocks and the solar activity that is generally



thought to be the origin of the entire phenomenon as well as the larger-scale disruptions in solar wind that they are a component of. This article will make use of the following phrases and terms: A disturbance in the solar wind is defined as any change on a large scale to the characteristics of the solar wind in its normal or calm state. A shock wave is a disturbance in the solar wind that has a shock at the leading edge of the disturbance. Both Wilcox (19691) and Hundhausen (1996) provide reviews that discuss these occurrences in some detail.

### **A QUALITATIVE DESCRIPTION OF SOLAR WIND DISTURBANCES**

Traditional solar-terrestrial research suggests that there are two types of interplanetary disturbances: those that are transient and occur after certain solar flares, and those that are recurrent and occur at a distance of one astronomical unit and are thought to be caused by long-lived active regions (also known as "M regions"). In this section, we will present qualitative descriptions of how these two different kinds of disturbances interact with a constant, spherically symmetrical, ambient solar wind, which will ultimately lead to the formation of shocks. Having these descriptions at hand makes it possible to better manage shock data as well as quantitative theoretical models.

#### **Flare-Associated Solar Wind Disturbances**

The violent expulsion of matter is caused by large solar flares, which can be observed in the visual, radio, and particle spectra. Let's imagine that this material, which is most likely plasma originating from the chromosphere or the low corona, fills a volume and accelerates outward into the slower solar wind. Figure 2 depicts what could be a piece of the disruption that occurs in the solar wind as a result of the solar wind's journey into deep space. This disruption would occur in the solar equatorial plane. Later sections provide theoretical and observable reasons for this effect, which implies some lateral expansion of the shape produced by the disturbance in the drawing. These arguments are provided so that the phenomenon can be understood. Flare ejecta have to expand, which causes the plasma in the solar wind to become more compressed and pushes magnetic field lines out of the way (the high electrical conductivity of the plasma prevents the plasmas from quickly penetrating one another). If the speed of the ejected material is faster than the local sound speed (also known as the Alfvén speed), then a shock front will develop at the leading edge of the compressed ambient plasma shell.

The specifics of the flare process can have an effect on the nature of the transition zone that exists between the compressed solar wind in the ambient space and the ejecta from the flare. If the location of the flare was also a generator of the ambient solar wind, then the magnetic

field lines in the plasma surrounding the flare must have connected to the background field. However, as shown in Figure 2, this connectivity is only present on a very small portion of the border that can be seen directly above and to the right of where the flare was. The majority of the boundary surface is responsible for separating solar plasmas that come from distinct source regions and have different histories. As a consequence of this, the substance on either side of the border may display thermodynamic and chemical features that are notably distinct from one another. Because magnetic field lines are unable to pass through such an area of the boundary, there must be a tangential break in the plasma and magnetic field that permeates the space between the planets. A tangential discontinuity can be expected across the entire boundary surface if the flare zone is not a source of the ambient solar wind. This is significantly different from the scenario presented for a spherically symmetric wave, in which the field lines traverse the entire boundary. If the flare region is not a source of the ambient solar wind, then a tangential discontinuity can be expected across the entire boundary surface. Because of the tenuous nature of the interplanetary plasma, diffusion in the direction normal to magnetic field lines is excruciatingly slow. Collisions are extremely rare. Any changes in thermodynamics or chemistry that occurred between the ambient plasma and the flare plasma would be preserved as a result of the expected tangential character of the boundary discontinuity.

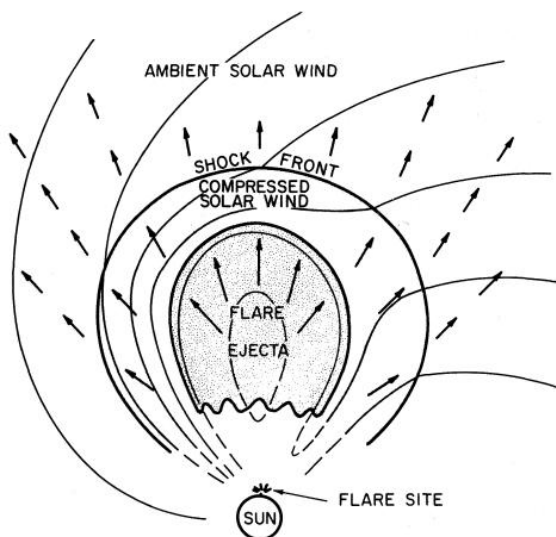


**Figure 2.** A rough equatorial cross-sectional drawing of a solar wind disturbance caused by a flare and its subsequent interaction with the ambient solar wind, as in figure 1. Once again, the arrows and glowing lines denote the speed of the plasma flow and the magnetic field, respectively. An arrangement symmetrical about the flare spot has been drawn, but the sun's rotation has been disregarded.

The particulars of the process by which the flare is produced have a significant impact on the magnetic field and plasma structure contained within the flare ejecta. Because there is a current sheet that runs through the core of the ejecta as well as along its border, the magnetic field lines have to reconnect at the flare site. This prevents any diffusion of the plasma with regard to the field lines as well as any "reconnection" of the field lines. As can be seen in figure 3, the Sturrock 119671 flare model assumes and creates magnetic field configurations that make reconnection a very real possibility. This is because certain theories of solar flares employ this process as the primary mechanism behind the flare. A reconnection of this kind would lead to the formation of closed magnetic loops within the plasma of the flare, as seen by the field line with dots in Figure 2.

Gold has made a case for why this agreement should be made. If some of the material that is being ejected from the flare is moving outward at a higher pace than that which is occurring at the tangential discontinuity (due to acceleration on the part of the former or deceleration on the part of the latter), then a second shock may emerge within the flare ejecta. This would be considered a "reverse" shock since it would be moving away from the sun in reference to the plasma while at the same time being convected outward by the fast plasma velocity.

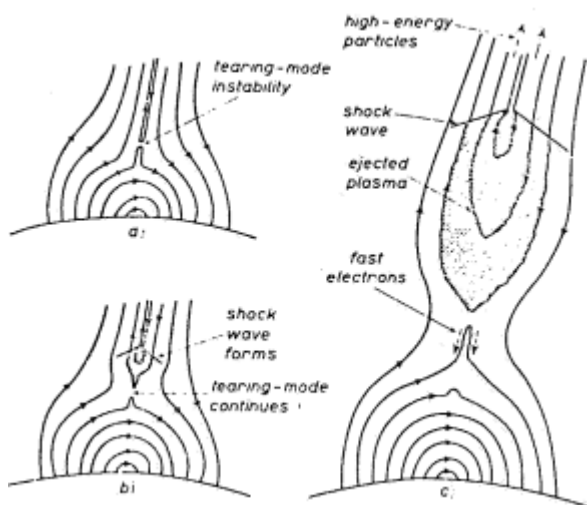


**Figure 3. In the Sturrock [1967] solar flare model, many configurations of the coronal magnetic field are shown. The principal source of energy for this model is called field line reconnection, and it is responsible for creating closed magnetic field loops inside of the flare ejecta (c).**

Solar wind that is constantly gusting and picking up speed It has been demonstrated that certain high-velocity solar wind streams have been present over numerous solar revolutions. These streams are thought to have originated in different regions of the sun's activity. Take,



for instance, the solar wind, which is constantly moving in a direction that is radially outward from the sun at a very high speed. Figure 4 depicts what would appear to be a hypothetical cross-section of this stream if it were cut through the solar equatorial plane as viewed from the rotating reference frame of the sun. Archimedes spirals are characteristic of the flow when viewed from this angle, and the magnetic field lines are seen to follow the streamlines of the flow (as shown in figure 1(b)). Assuming there is a gentle breeze blowing in front of the swift stream, its flow will be in more tightly wound spirals, and it will eventually collide with the rapids. Again, the high electrical conductivity of the plasma prevents it from penetrating one another; as a result, the ambient plasma needs to be compressed and redirected before it can flow in a path that is parallel to the contact with the fast stream. If the inflow of ambient plasma relative to this interface is quicker than the local sound speed, then a shock wave should form at the front of the compressed ambient plasma region. This will cause the ambient plasma to expand. The resulting flow pattern is one that maintains its consistency inside a reference frame that circles around the sun. Figure 5 illustrates this pattern as though it were observed from a stationary vantage point; from this perspective, the entire shock wave appears to rotate anticlockwise around the sun.

The magnetic field and plasma structure of this shock wave are quite comparable to those of disruptions induced by flares. Once more, there should be a tangential discontinuity at the border between the compressed ambient solar wind and the high speed stream that separates the plasma and magnetic fields that originate from two distinct solar source regions. Again, it is possible to predict distinct thermodynamic and chemical properties on either side of the boundary, and these differences will remain as long as there is a slow rate of diffusion across the field lines. If matter is flowing towards the tangential discontinuity, there is a possibility that the high-velocity stream will experience a second shock in the opposite direction.

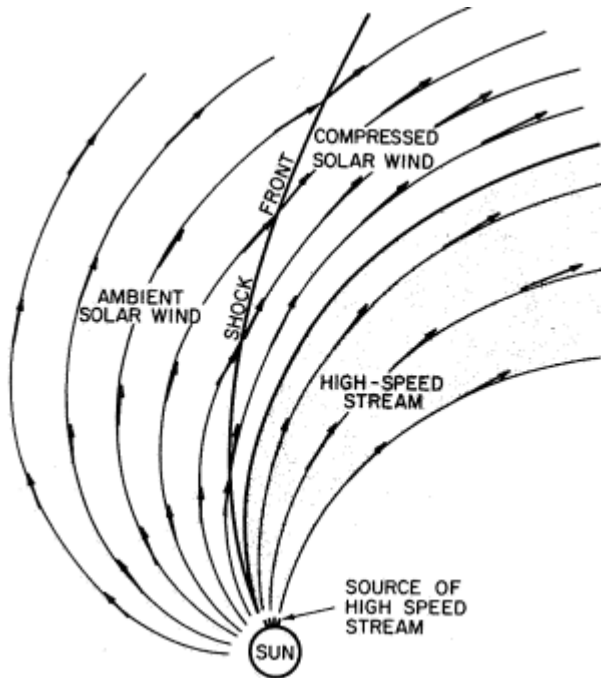


**Figure 4.** An equatorial cross-sectional depiction of the high-speed solar wind stream depicted in Figure 1 interacting with the slower solar wind in the background. A frame of reference orbiting the sun illustrates the interaction. Once again, the arrows and glowing lines denote the speed of the plasma flow and the magnetic field, respectively.

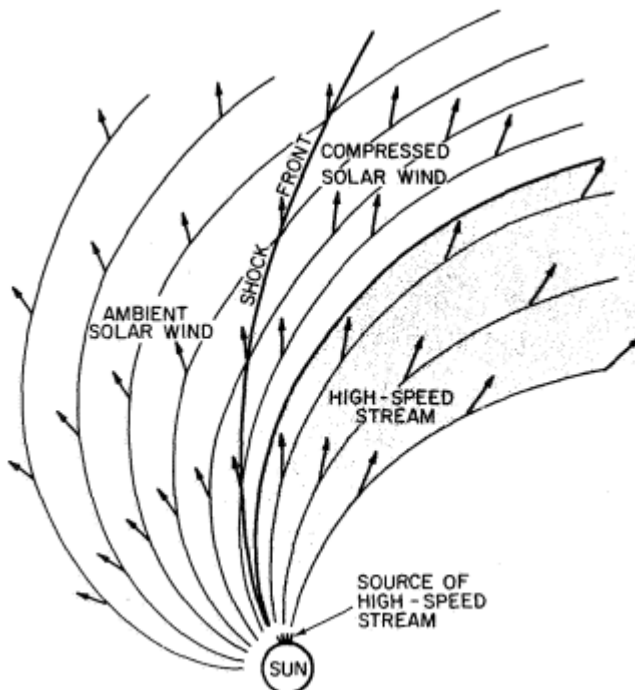


**Figure 5.** Figure 4 shows the interaction in question from a fixed viewpoint.

### Differences Between Solar Wind Turbulence Caused by Flares and That Caused by Steady Streams



A disturbance in the solar wind that is associated with a flare is depicted in Figure 2, and a disturbance in the solar wind that is connected with a continuous stream is depicted in Figure 5. The shape of the shock front is the one that stands out the most among these. Those shock fronts that are connected with steady streams have a tendency to be closely aligned with the spiral interplanetary field lines, but those that are connected with flares have a tendency to be radially symmetrical. Either the observation of a single disturbance by a large number of widely spread spacecraft or the observation and statistical analysis of a large number of shock orientations by a single spacecraft might be used to differentiate between these two geometries [Hirshberg, 1968]. Another distinguishing feature is the fundamental construction of the field lines that cut across the shock front. During a disturbance that is connected with a flare, field lines in the preshock and ambient plasma all point outward into interstellar space. On the other hand, during a disturbance that is associated with a steady-stream, these same features point back towards the sun. There is a possibility that high-energy measurements of galactic cosmic rays, which are able to monitor the form of magnetic fields across enormous distances, would be able to differentiate between the two topologies.

When pursuing either of the tests proposed below, as is done in the following section, keep in mind that these two sorts of interruptions are extreme situations. Classes in the centre, in which solar plasma is emitted for approximately the same duration of time as its transit to an observer, are possible and should reveal configurations that fall somewhere in the middle of the two extremes. A link of this essential kind has been discovered by Bumba and Obridko [1969] between solar flares and the locations of the sources of high-velocity streams. This correlation was found between solar flares and high-velocity streams. The absence of symmetry in the ambient medium would cause the transient disruptions caused by such flares to be distorted into a form that is considerably different from that seen in figure 2. In the following, we will present some evidence that the perturbations in the solar wind that at first glance seem to be associated with flares actually reflect certain characteristics of steady-stream emission.

### **THEORETICAL MODELS OF SOLAR WIND DISTURBANCES**

Quantitative theoretical modelling has been done on some of the qualitative aspects of the solar wind disruptions that were discussed before. Because comparable models have been previously explored in substantial depth [Hundhausen, 1970b; Hundhausen and Montgomery, 1971], this article just presents a brief discussion of some intriguing results. Under the presumption of spherical symmetry, the majority of previous research has concentrated its



efforts on determining how shock waves associated with flares travel through space. The high thermal conductivity of interplanetary electrons will be explored in relation to both classes of solar wind disturbances, as well as the propagation of nonspherical, flare-associated shock waves and the formation of shock waves in steady-stream disturbances. Also included in this discussion will be the propagation of nonspherical, flare-associated shock waves and the generation of shock waves in steady-stream disturbances.

### Flare-Associated Shock Waves

If the background medium and the disturbances are assumed to be spherically symmetric (plasma properties are, as a result, just functions of the time  $t$  and the heliocentric distance  $r$ ), then it is not difficult to develop theoretical models of transient disturbances propagating through an ambient solar wind. To construct spherical shock wave solutions of the adiabatic fluid equations, Parker [1961, 1963] used similarity techniques, assuming fundamental dependence on the parameter  $\eta = tr^{-\lambda}$ . Any feature of these solutions that is at position  $r_0$  at time  $t_0$  moves with time as  $r = r_0 (t/t_0)^{1/\lambda}$ . The solutions are connected to the medium that is all around them by supposing that there was a powerful shock at the forefront of the disturbances.

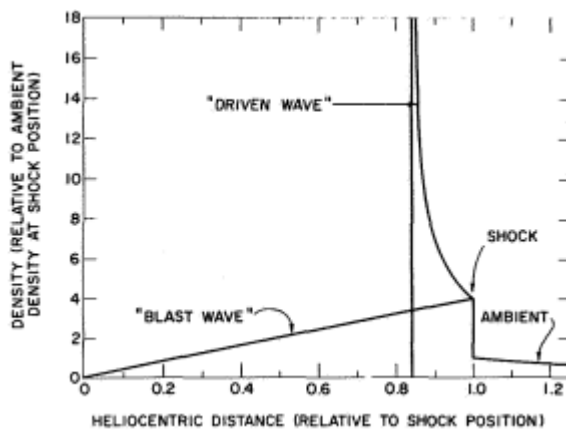


**Figure 6. Solar wind shock waves with a spherical symmetry can be propagated using similarity solutions. In contrast to the blast wave, whose energy remains constant over time, the energy of the "driven wave I" increases linearly with time.**

Figure 6 displays a scatter plot of two of Parker's shock waves, each of which has a ratio of specific heats equal to  $5/3$  and an ambient density that is proportional to  $r^{-2}$ . The scatter plot is normalised to the location of the shock  $r = r_0$ . Assuming that an infinite shock strength is represented by a factor-of-four shift in density at the shock site. The solution that corresponds to this problem is called driven wave  $\lambda = 1$ . After the first shock, the density continues to gradually climb until it suddenly reaches its maximum  $r \rightarrow 0.84$  a point of reference for the



location of the vertical line on Figure 6. This wave moves at a constant speed, and one can demonstrate that its energy increases in a linear fashion over the course of time. The "piston" can be located at the singularity, and it is responsible for propelling (or driving) the wave ahead. The explanation for "blast wave" is as follows  $\lambda = 3/2$ : Following the shock, there is a consistent and ongoing reduction in density. This wave's speed decreases throughout the course of time, but its energy remains the same. The wave that it represents was caused by an explosion that occurred at  $r = 0, t = 0$  without the need for any further activation after that point. The characteristics of the wave, such as its shock speed and the amount of time it takes to travel to a given radius, are only dependent on the total energy that the disturbance possesses. This is the case for "blast wave" solutions, which are approached by disturbances with energy input occurring over a period of time that is relatively short in comparison to the amount of time it takes to travel to a position of interest. This is a feature that is both interesting and practical. When considering the disturbances caused by solar wind, it will be beneficial to keep in mind the terms "driven" and "blast" waves. The driven wave is a type of physical disturbance in which the features are determined by the sunward-bound originating signal, whereas the blast wave is a type of physical disturbance in which the characteristics are determined by its interaction with the medium that is all around it.

Parker's fundamental similarity solutions have been extended by derived similarity solutions, which are valid to first order in the ratio of the ambient solar wind speed to the shock speed but do not require the premise of infinite shock strength. These derived similarity solutions have been developed so that Parker's fundamental similarity solutions can account for more complex situations. These parallels between interplanetary shock waves and other phenomena serve as the foundation for a number of different theories. According to observations (which will be explained in the following section), the majority of shocks that occur between the planets are found to be of an intermediate strength. As a result, the solutions that are analogous may or may not be relevant to the cases involving solar wind.

Using numerical integration of the fluid equations, it is possible to find a solution to this problem for shocks of any given magnitude. Consequently, spherical wave solutions of the adiabatic fluid equations were found by Hundhausen and Gentry [1969a, 1969b] (once again ignoring magnetic forces but taking solar gravity into consideration). A plot of density against volume is shown in figure 7.

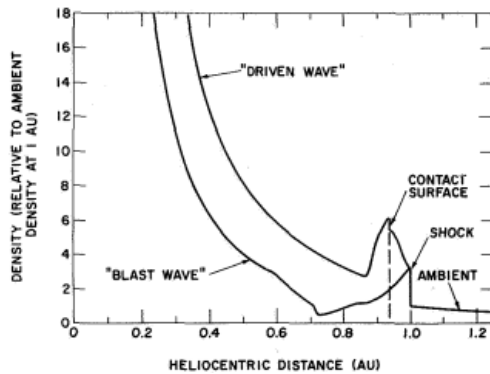


**Figure 7. Propagation of spherically symmetric shock waves in the solar wind: numerical solutions. Figure 6 [modified from Hundhausen and Gentry, 1969a] uses the same fundamental definitions for the "driven wave" and the "blast wave" situations.**

coordinates in the heliocentric system (in astronomical units) for two of these shock waves, as well as a specific heats ratio  $\gamma = 5/3$  an adiabatic solar wind blowing at a speed of 400 km/s in the background,  $\text{sec}^{-1}$  and a density of 12 protons  $\text{cm}^{-3}$  at 1 AU. The fact that the shock site had a density shift of less than a factor of 4 is an indication of the limited power of the shock. The driven wave solution demonstrates a continual increase in density behind the shock until a contact surface is achieved. This contact surface differentiates the compressed ambient solar wind from the gas that was discharged in the initial disturbance at time zero. Figure 7 only gives a qualitative representation of the elements of this interface, which means that additional thought needs to be given in order to integrate the numbers correctly. There is a density singularity at the "piston" interface, but similarity solutions don't have one (it appears that this is because similarity solutions assume a temperature of zero). The wave travels at a pace that is almost constant, and its energy increases in a linear fashion as time passes. Similarity theory compares it to the driven wave, which depicts a wave that is being propelled by the sun's constant production of driving petrol (forming a new steady state; see image  $r < 0.83 \text{ AU}$ ). It is important to take into account the flow that occurs within the heliocentric distances of the contact surface, which is different from the similarity solution that is presented in Figure 6. Figure 7 is an illustration of the numerical solution known as the blast wave. This solution displays a steadily falling density for a length of time after the shock, before rising to the initial ambient profile in a manner that is roughly proportional to the amount of time that has passed since the shock ( $r^{-2}$ ) at  $r \approx 0.6 \text{ AU}$ . This wave eventually becomes more sluggish but keeps the same total quantity of energy throughout its progression. Therefore, it is comparable to the blast wave of the similarity theory, which depicts a wave that is produced by an explosion and has a short duration at time  $t = 0$ ,



followed by, in this case, a return to the conditions that were there before the explosion. [Hundkausen and Gentry, 1969a] found that the properties of a certain sort of wave that spontaneously generates are completely related to the total energy that is present in the disturbance. This finding is comparable to the similarity hypothesis. In contrast to the predictions made by the similarity theory, the density rarefaction that occurs in the numerical blast waves as a result of the shock does not travel all the way back to the sun.

Figure 8 presents a more in-depth comparison of the driven wave solutions created numerically by plotting density (normalised here to the ambient density at any heliocentric radius) vs heliocentric position (normalised to one at the leading-edge shock). This comparison was made by plotting density (normalised here to the ambient density at any heliocentric radius). Both solutions demonstrate a new constant flow at small heliocentric distances. This flow is faster than the flow near to the contact surface that separates the ambient gas and the "driving gas." Both answers entail a "reverse shock" within the driving gas, which can be found at  $S_z$  in the numerical solution and at the innermost  $S$  in the similarity solution. This is something that was mentioned in the qualitative debate that came before it. demonstrated that this configuration will only be observed at a certain heliocentric position in interplanetary space if the solar disturbance that produced the shock wave lasted for longer than 10% of the shock wave's transit period. This is the only condition under which this configuration can be observed.

The vast majority of solar flares' visible radiation is confined to a region smaller than the entire Earth. Therefore, the theoretical models listed above, all of which presume spherical symmetry of the disruption in the solar wind associated with flares, are all incorrect.

## **METHODOLOGY**

It has been demonstrated that severe shock waves, such as the Earth's bow shock, which has a typical magnetosonic Mach number of 8, have a different temperature and density structure than the magnetic field. This is the case even though the magnetic field is susceptible to higher levels of perturbing changes. In the case of minor interplanetary shocks with magnetosonic Mach values in the range of 1–4, less conspicuous plasma trails are usual, and the magnetic field is once again able to suppress large disturbances. For a more accurate depiction of these less significant occurrences, it is necessary to take into account both the fluctuations brought on by the solar wind and those brought on by shocks. These fluctuations and shocks are both brought on by the dissipation effects of the thin dissipation layer. A difficulty that has been around for a long time is identifying which regions are upstream and



which are downstream in order to use them in the computation of shock parameters. This issue has come up at than once in connection with the Bn calculations, and measurements of the magnetic field with a better temporal resolution have been essential in giving the leeway that is required to finish the study. When attempting to determine features of plasma, such as temperatures in close proximity to shock waves, additional complexities arise. This may be more challenging in the outer heliosphere, where circumstances of cold plasma predominate, and as a result, caution must be made while selecting suitable parameter values.

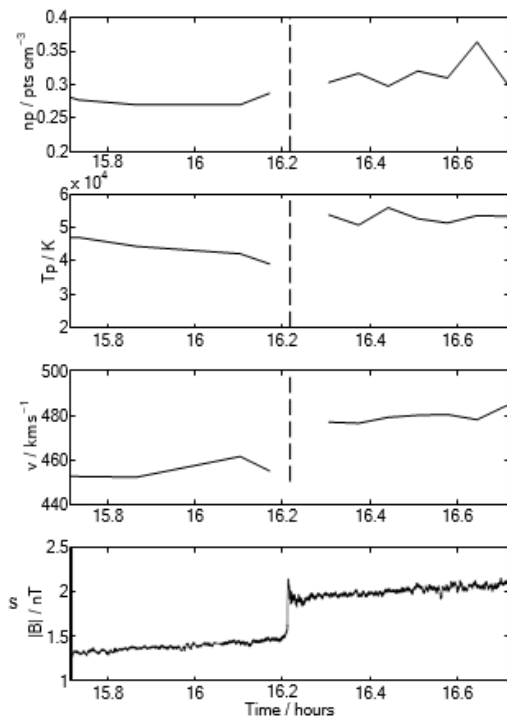


**Fig. 8. Example of a low rB shock that took place on day 128, 1998, displaying proton density (the top panel), proton temperature (the second panel), proton bulk velocity (the third panel), and magnetic field magnitude (the bottom panel).**

The Ulysses spacecraft saw approximately a hundred different interplanetary shock waves between 1996 and 1999, and those observations are analyzed here. Local shock parameters are determined by meticulously applying a set of upstream and downstream regions to all of the shocks. The plasma zones' sizes have been determined as a balance between allowing for sufficient so- lar wind fluctuations and not being overrun by those produced by the shock. The shock parameters are then compared to the theoretical requirements. It is shown that the choice of data utilized in the research and the assumptions made about the thermodynamic characteristics of the solar wind plasma have a significant impact on the degree to which certain shock parameters match with the theory. The challenges of determining the plasma temperature in a collisionless plasma have implications for the selection of data that may be



utilized for the study. One possible explanation for the gap between the analysis and theory is that the events employed here are very faint interplanetary shocks.

## DATA ANALYSIS

For this experiment, we made use of the Ulysses shock list and its associated shock waves. Since Ulysses was at its most distant position from the Sun during this period, its polar orbit carried it below the ecliptic plane. This occurred because Ulysses was at its most distant point from the Sun. Ulysses has been following an orbit with a period of 6.2 years and an inclination of 79.4 degrees with regard to the ecliptic plane ever since it passed Jupiter in 1992. It is necessary to observe a rapid shift in the amplitude of the magnetic field over the course of a few seconds in order for a shock to be put on the shock list. In addition to this, the bulk velocity of the plasma must experience a corresponding rise or reduction. Due to the lower temporal resolution of the plasma measurements, it is not possible to monitor fluctuations in the plasma parameters on the same time scale as the magnetic characteristics. This is because of the magnetic parameters. This is due to the fact that monitoring plasma has a lower temporal resolution than other types of measurements. When compared to the frequency at which magnetometer data is acquired, plasma parameters are produced every 4 or 8 minutes. The high time resolutions of the data presented challenges in a previous research (Balogh et al., 1995), which attempted to analyze the interplanetary shocks seen by Ulysses between the years 1990 and 1993. Already, the estimated Mach numbers and low  $rB$  values (some of which are less than 1) demonstrate that the interplanetary shocks that are the subject of this investigation are fairly feeble structures. The preceding research provided conclusive evidence for this assertion.

The resolution of the plasma data has an effect, at least to some degree, on the size of the upstream and downstream areas that are to be employed in the computation of the shock parameters for this investigation. To build a plasma state that is indicative of the whole, data points on the plasma are gathered from two distinct locations regardless of the temporal accuracy, and magnetic parameters are selected from data that spans ten minutes on each side of the shocks. This allows for the generation of a state that is representative of the plasma as a whole. In this investigation, the magnetic parameters that were calculated include  $B_n$ , which is the angle that exists between the shock normal vector and the upstream magnetic field;  $B_{dn}$ , which is the angle that exists between the shock normal and the downstream magnetic field; and  $rB$ , which is the ratio of the magnitude of the downstream magnetic field to the magnitude of the upstream magnetic field. The magnetic coplanarity theorem is used in the



calculation of the shock normal, as well as  $B_n$  and  $B_{dn}$ . It has been concluded that the utilization of 10-minute averages of upstream and downstream areas is sufficient for the purposes of this inquiry. This conclusion was reached on the basis of the findings of a statistical method that was used to determine  $B_n$ . When  $B_n$  was computed using the statistical method, it became obvious that this was the case. Both Figure 1 and Figure 2 display two examples of shocks, one with a low  $r_B$  value and one with a high  $r_B$  value. The temporal resolution of the magnetic data is significantly lower compared to that of the plasma data. Even while the magnetic shock signature is present in both the weak and the strong case, it is abundantly evident that in the scenario with low  $r_B$  the plasma transition is far less noticeable than in the situation with high  $r_B$ . This is something that is immediately obvious to each and every person. Calculations for a variety of plasma-related parameters, including the Alfvén number, the magnetosonic Mach number, and the downstream-to-upstream entropy ratio, need the presence of plasma data. In a stationary reference frame that is perpendicular to the shock front, the Mach number indicates the relative speed of the plasma in comparison to the speed of a certain linear wave. These velocities are measured in a direction that is perpendicular to the path of the shock front. Without initially computing the requisite shock velocities, it is impossible to determine these Mach numbers.

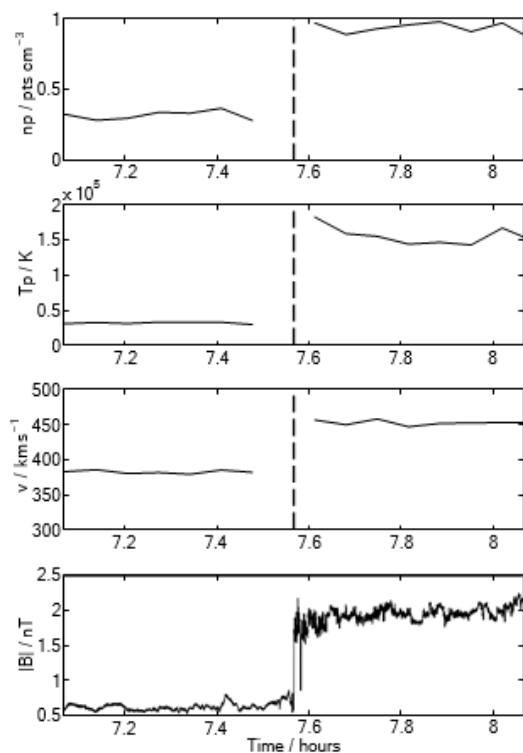




**Fig. 9. Example of a high rB shock that occurred on day 146, 1999, displaying the proton density (top panel), the proton temperature (second panel), the proton bulk velocity (third panel), and the magnetic field magnitude (bottom panel).**

Method developed by Smith and Burton (Smith and Burton, 1988). For the purpose of determining whether or not there is a rise in entropy throughout the shock waves, the equation (1) shown below is utilized. The ratio of the entropy argument's downstream to upstream contributions may be calculated by dividing the right-hand side of Equation 1 by its

left-hand side.  $\left(\frac{T^{1/(\gamma-1)}}{n}\right)$  However, the reasoning presented by this statement is utilized in this work. T and n represent the temperature and number density for each of the particle species, and represents the ratio of specific heat capacities. Equation (1) is written for a three-component plasma that is composed of protons, which are denoted by the subscript p, alpha particles, which are denoted by the symbol, and electrons, which are denoted by the symbol e. The upstream region is denoted by the subscript u, while the downstream region is denoted by the subscript d..

$$\frac{n_{pd}T_{pd} + n_{ed}T_{ed} + n_{\alpha d}T_{\alpha d}}{n_{pu}T_{pu} + n_{eu}T_{eu} + n_{\alpha u}T_{\alpha u}} > \left(\frac{n_{pd} + n_{ed} + n_{\alpha d}}{n_{pu} + n_{eu} + n_{\alpha u}}\right)^\gamma$$

In the past, calculations of entropy at shock waves have only received a limited amount of attention. In point of fact, the hypothesis that shocks recorded in this manner will result in an increase in entropy has been used as a test in the identification.

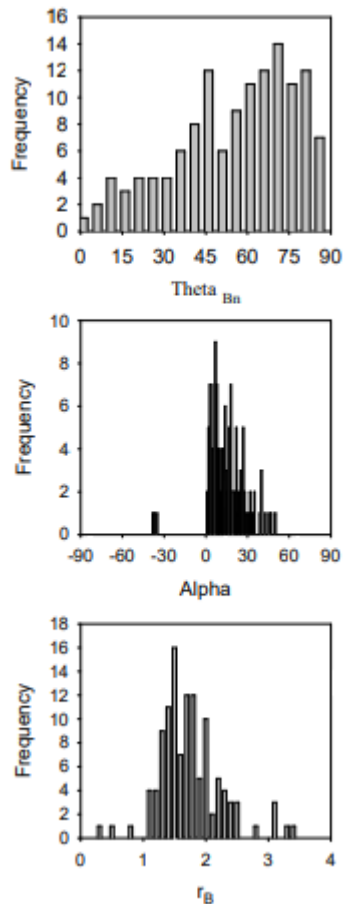


**Fig. 10.** The magnetic characteristics for all of the shock waves that were taken into consideration for this survey utilizing the magnetic coplanarity approach and using a 10-minute average of the data for both the upstream and downstream areas.

Histogram of the values of  $B_n$  is displayed in the top panel. Histogram of the magnetic deflections may be found in the middle panel. Histogram of magnetic compressions may be seen in the bottom panel..

Magnetic compressions can create shockwaves. For instance, Richter et al. (1985) used a formula quite similar to Eq. (1) for this very purpose. Before this, Chao (1973) used a two-component plasma formulation that contained the simplifying condition of quasi-neutrality to analyze nonlinear wave steepening in the solar wind. In every case where the shock parameters were computed, as described above, the magnetic parameters were found to be consistent with the theoretical expectations. Specifically, this means that the magnetic field deflections are happening as expected, and that the measured values of  $r_B$  are consistent with those expected for both rapid and slow mode shocks (as mentioned in the Introduction). For all of the considered shock waves, a histogram of their  $B_n$  values, deflections, and magnetic compressions is shown in Figure 3. The magnetic deflections are determined by a variable



equal to the difference between  $B_{dn}$  and  $B_n$ . The type of shock waves that can be predicted to exist at the distances from the Sun where Ulysses is detected are quasi-parallel shock waves. There are more quasi-perpendicular shock waves than quasi-parallel ones, as seen by the histogram of  $B_n$  values in the upper panel. Deflections are shown to be positive for all but three events in the central panel.

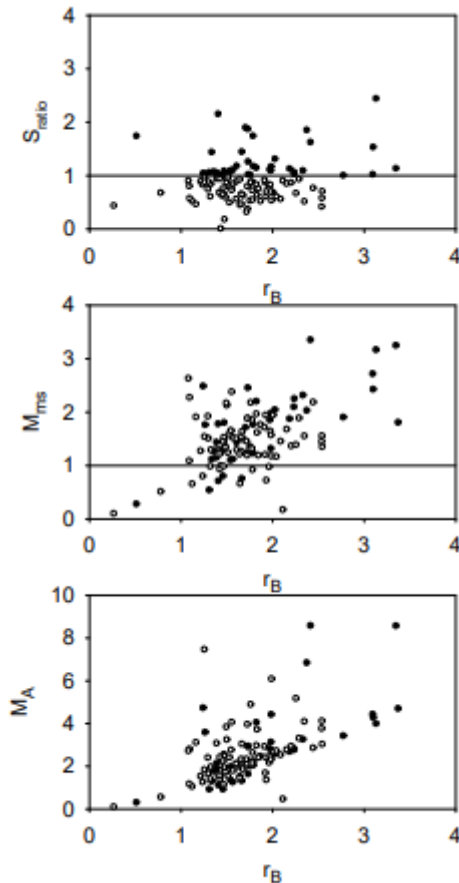


**Fig.11** These findings are based on data from two plasma points upstream and downstream for a three-component plasma with  $\beta = 5/3$ . The entropy ratio vs  $r_B$  is displayed in the upper panel, the magnetosonic Mach number versus  $r_B$  in the middle panel, and the Alfvén Mach number versus  $r_B$  in the lower panel. Entropy always grows in closed circles and decreases in open ones..

In the bottom panel of Figure 3, a histogram of magnetic compression ratios shows that all of the shock waves are fast modes, with the exception of three occurrences. These three instances are shown to be the exceptions. There are three potential slow shocks that stick out, and they all have negative deflections and  $r_B$  values that are less than one. Despite the fact that the calculated magnetic parameters are compatible with the theory, it seems that certain shock waves do not appear to follow the expected findings in terms of Mach numbers and



entropy ratios. This is the case despite the fact that the theory accounts for all of the magnetic parameters. Calculations of entropy performed on a plasma consisting of three components, using the assumption that  $\beta = 5/3$ , generate the unexpected results that are presented in Figure 4. In this section, we take the average of the two temperatures for protons that may be found in the SWOOPS data. These temperatures are derived using different methodologies, although they typically fall on opposite sides of the actual temperature of the proton. The method that has a tendency to provide inaccurate estimates of the proton temperature is the integral over all energy channels and angular bins in the three-dimensional velocity distribution space. The temperature of the proton may also be determined by utilizing the radial component of the temperature tensor, which involves the addition of values across all of the angular bins while maintaining the same amount of energy.

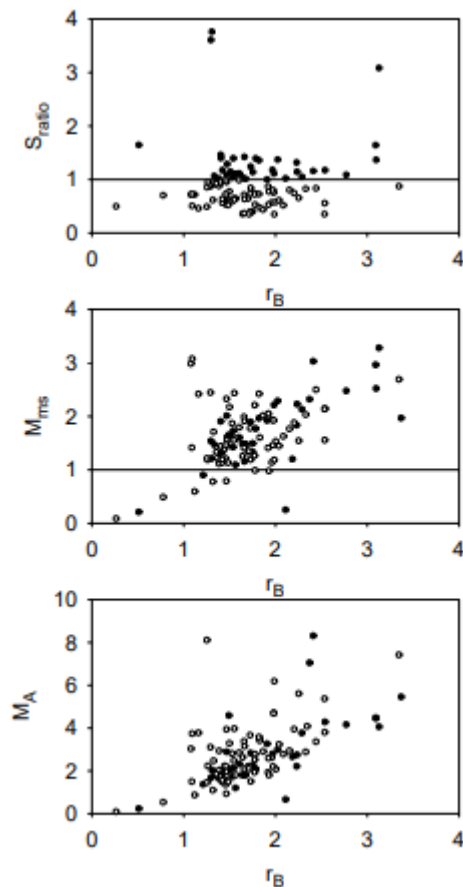


**Fig. 12. For a 3-component plasma and  $\beta = 5/3$ , these outcomes are achieved using up and downstream data periods of 1 hour.**

The entropy ratio vs  $r_B$  is displayed in the upper panel, the magnetosonic Mach number versus  $r_B$  in the center, and the Alfvén Mach number versus  $r_B$  in the lower panel. The entropy of closed circles is greater than that of open ones. The temperature of the particles is



not evident in the plasma data and cannot be inferred from the distribution functions. Here, the particle temperature is represented by the Liu et al. (1995)-determined empirical relation  $T = 3.9T_p$ . The most surprising finding in Fig. 4 is that entropy appears to decrease across the borders of over half of the shock waves..

The next phase in the inquiry is to attempt to locate the cause of the apparent entropy drop problem. Considering the fact that the entropy is anticipated to rise from upstream to downstream for every shock waves, this is the next step in the investigation. It is probable that the 10-minute upstream and downstream zones, which have been discovered to be acceptable for analyzing interplanetary shock waves in terms of magnetic characteristics, are too short for the plasma parameter study. This is something that has to be investigated. If this is the case, then the rise in entropy that occurs at these shock waves could not become apparent until far longer periods of time have passed. Entropy ratios have been estimated using 1-h upstream and downstream areas in order to look into the probability of this happening. In this round of computations, the average of the two estimates of the proton temperature rapture was used. Additionally, an upstream and downstream adiabatic condition

was assumed.  $\gamma = \frac{5}{3}$  plasma that contains and is meant for use with three separate components. Figure 5 is a representation of the resultant entropy ratios, which makes it abundantly clear that increasing the amount of time spent upstream or downstream does not alleviate the entropy issue.

Researchers have demonstrated, through the process of monitoring the temperatures of electrons throughout the shock waves, that electrons frequently defy expectations by not heating adiabatically. This finding was made possible by using the temperatures of the electrons. When just the electron heating that is anticipated to result from adiabatic compression is taken into consideration, there are seventy-five instances in which the downstream temperature is not high enough to be within ten percent of the value that was projected. Due to the fact that the conservation of the magnetic moment was seen, 103 out of 104 samples did not achieve the electron temperature that was predicted to be obtained. The margin of error for this finding was 10%. It has been shown through calculations that during 39 out of the 50 shocks, in which the entropy reduces, the electrons give the appearance of being cooler. Due to the particular wind conditions that were seen by Ulysses during the time period under investigation (private mail from B. Goldstein, JPL, dated 13 March 2001), it is possible that the electron parameters presented in this article are not always trustworthy. The



significance of bringing attention to this reality cannot be emphasized in any way. The fact that this was the case should also be emphasized. The decision that was taken is yet another component that has the potential to influence these findings. According to the findings of Totten and Freeman (1995), a number that is closer to 1.5 is more suited for the solar wind. This figure for was determined by utilizing data from Helios 1 in an empirical calculation. In the end, the radial temperatures may be more precise approximations of the proton temperatures than the angular resolutions are (private letter, J. Gosling, LANL, May 21, 2001). This was stated in J. Gosling's research at LANL on May 21, 2001. This was discovered as a result of an inquiry that J. Gosling and his fellow employees conducted at LANL. The temperatures that may be found in the radial portions are consistent with the lower of the two proton temperatures that were discussed before. When these two figures were added together, the resulting number was the average temperature, which was then utilized to calculate the findings shown in Figure 4. We were only provided with proton measurements, radial proton temperatures, and a multiplier of 1.5 in order to perform the calculation for the shock parameters. Figure 6 illustrates these findings, which demonstrate that the majority of the shocks in this scenario have seen an increase in entropy, with just 14 shocks sitting slightly below the boundary. These results suggest that the majority of the shocks in this scenario have witnessed an increase in entropy.

It has been demonstrated that selecting data meticulously can cut down on the number of shock waves that are unable to pass the entropy test for a shock wave. Using the empirical value of 1.5 increases the number of shock waves for which an increase in entropy is projected beyond their borders; nevertheless, from a physical point of view, it is not immediately clear whether or not this is the proper thing to do. A heating effect that may be identified in the solar wind can provide an explanation for the disparity that exists between the empirical value and the adiabatic value. It should not come as a surprise that the solar wind will see a drop in temperature as it travels through the heliosphere. This gap may be explained by a hot population of electrons streaming down the heliospheric magnetic field lines straight from the corona. The cooling is less than what is anticipated from adiabatic expansion, and this discrepancy may be explained by adiabatic expansion. The cause of this is a flux of electrons that generates heat.

On a size comparable to the heliosphere, these processes are responsible for the characteristics of the plasma that constitutes the solar wind. Our recently acquired information informs us that the empirical value of is unsuitable for use in the investigation of



shock waves, and that instead, we require a value that characterizes the properties of the plasma in the vicinity of a shock wave. This information was obtained through a recent discovery. Theoretically, we should anticipate far higher amounts of  $\gamma$  are thought to:

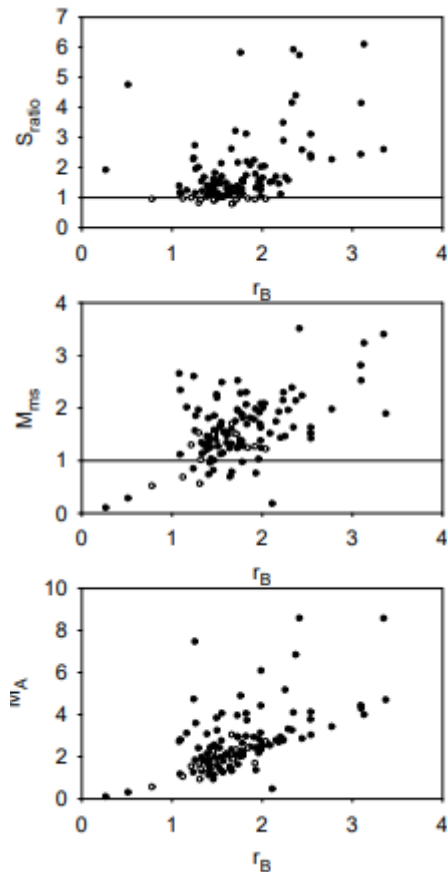


**Fig. 13.** These findings were achieved by utilizing just proton data, two plasma points to measure upstream and downstream data periods, and a value of  $\gamma = 1.5$ .

The entropy ratio is plotted against  $r_B$  in the top panel, the magnetosonic Mach number is plotted against  $r_B$  in the middle panel, and the Alfvén Mach number is plotted against  $r_B$  in the bottom panel. Entropy grows in circles that are filled in, whereas entropy reduces in circles that are open..

The condition of the plasma in the places that are near to the shock waves. Theoretically, values for  $\gamma$  of 2 (Chao and Wiskerchen, 1974) or 3 (Papadopoulos, 1985) have been justified; nevertheless, applying these values to the data would result in a significant increase in the number of shock waves, creating the impression that their entropy has reduced.

One may think of an explanation for the estimated decreases in entropy that take place at some interplanetary shock waves if it could be proven that one component of the shock structure extends beyond the confines of space. In this specific situation, the free energy that



is injected into the plasma at the boundary of the shock wave is unable to be instantly entirely thermalized. This is because the shock wave is moving at an extremely high speed. Because of this, temperatures further downstream would be lower than had been projected, and the spacecraft's sensors should be able to provide evidence of these affects. In general, the data on the magnetic field, and to a lesser extent, the data on the plasma, show that there is a reasonably definite border between the upstream and downstream states. This border can also be seen when looking at the data on the plasma. However, high frequency oscillations in the electrostatic field can disclose a trail that commonly lingers for several hours after it has been transported into the downstream zone. This can be the case if the field has been disturbed. It has been determined that these plasma waves, which are detected by the URAP sensor on board Ulysses, have frequencies ranging from 1 to 50 kilohertz and represent a significant part of the daily dynamic.

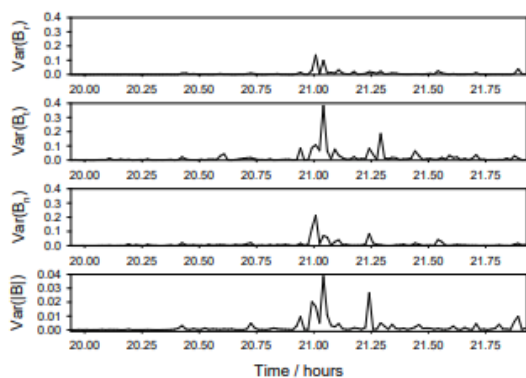


**Fig. 14. Variation of the magnetic field in three components and magnitude over four panels, based on data for shock collected every sixty seconds on day 326, 1996. The r, t, and n coordinates represent the three components in the conventional heliospheric r, t, and n coordinate system..**

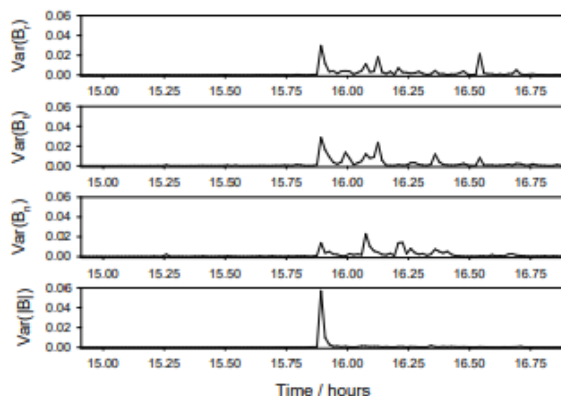




**Fig. 15. Variation of the magnetic field in three components and magnitude over four panels, based on data for shock collected every sixty seconds on day 296 in 1997. The r, t, and n coordinates represent the three components in the conventional heliospheric r, t, and n coordinate system.**

A variance analysis of multiple events has been carried out in order to assess the magnitude of shock structure present in the magnetic field data. This was done in order to find out more about the data. On each side of the shock waves, data regions consisting of one hour are collected, and the variance of each component as well as the magnitude of the magnetic field are computed utilizing sequential intervals of one minute's worth of data. The findings of this research are presented in Figures 7 and 8, respectively, for a shock that is quite powerful and that is either quasi-parallel or quasi-perpendicular. At the point when the shock transition occurs, there is a significant rise in both the variance of all three components and the amplitude of the magnetic field in each of these circumstances. When the scales of these two variance plots are compared, it is easy to see that the fluctuations in the three components of the quasi-parallel shock have far larger ranges than the magnitudes of either shock or the components of the quasi-perpendicular shock. This is evidenced by the fact that the quasi-parallel shock has a larger variance. The variation of the magnetic field is maintained at a higher level in the region that is further downstream.

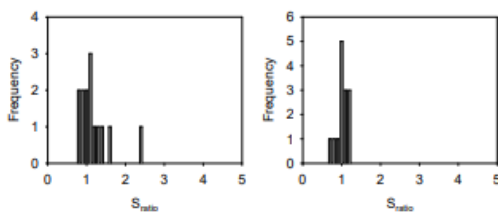


**Fig. 16. Histograms depicting the oscillations in entropy that occurred in the upstream and downstream areas of 2 shock waves after 1 hour.**

On the left is a picture of a shock that occurred on day 326, 1996 and had a rB value of 2.54. It showed that the shock entropy transition ratio was 2.33. Right panel: Shock with rB 1.56 on day 246, 1996 showing the shock entropy transition embedded in the background fluctuations in both cases, despite the fact that for the quasi-perpendicular shock, the fluctuations are almost entirely in the three-magnetic field components, whereas for the quasi-parallel shock, the fluctuations are in the magnetic field magnitude as well. In the case of the quasi-parallel shock, there is also enhanced variation in a brief region immediately upstream of the shock. This increased variance is a characteristic that is predicted due to the



geometry of the magnetic field. The analysis was also carried out for a mild shock that was quasi-perpendicular and quasi-parallel, although in both instances, the increase in variance was primarily restricted to the shock transition itself. According to the findings of the magnetic variance study, interplanetary shock waves have the potential to exert their influence over a substantial downstream region, but this is a quality that is only possessed by more powerful shock waves. This does not give any new information on the scope of the thermalization processes occurring at the weaker shock waves.

All of the earthquakes that are being looked at for this research are of a moderate to low magnitude, and some of them are of a very low magnitude. It is feasible for the surrounding entropy variations to have a considerable impact, particularly in the circumstances when the effect is the lowest. In order to illustrate the relative significance of these variations, entropy ratios have been computed for consecutive sets of two plasma data points ranging from one hour before to one hour after the passage of two shock waves. These calculations were carried out for a duration of one hour. The first occurrence is a shock of moderate intensity, whereas the second is a shock of lower intensity. Histograms of the entropy ratios that were obtained throughout the course of two-hour intervals are displayed as the outcomes of these computations in Figure 9. It is reasonable to anticipate that the entropy shift at the location of the shock wave will be easily distinguishable from the entropy changes in the surrounding area and will be of a greater magnitude. The entropy shift that occurred during the shock transition can be seen rather plainly above the distribution of background fluctuations in the panel on the left side of Figure 9, which displays the findings for the more powerful shock. On the other hand, the entropy shift that was brought on by the shock transition can be seen incorporated into the distribution in the panel on the right, which presents the findings for the milder shock. This demonstrates that in the case of shocks that are not as strong, the fluctuations in the background entropy are equivalent to the change in entropy that occurs during the shock transition. The significance of choosing upstream and downstream intervals of ten minutes for the calculation of entropy across the weaker shock waves is demonstrated by these results. This helps to guarantee that the computation is not obscured by the background fluctuation

## **CONCLUSION**

In this section, we will expound on those findings and try to make sense of them. Our research has led us to concentrate on the mechanism that is responsible for the nonadiabatic behaviour of the solar wind, which is something that we see in all of our models,



including the most basic one that deals with gas dynamics (1). We are able to account for this phenomenon by considering the behaviour of the aftershock temperature with respect to radial distance in addition to the high frequency with which shocks occur in the solar wind. To begin, let's look at a shock wave that moves through the solar wind.

## REFERENCES

1. Adhikari, L., Zank, G. P., Hu, Q., & Dosch, A. 2014, ApJ, 793, 52
2. Adhikari, L., Zank, G. P., & Zhao, L. 2021, Fluidika, 6, 368
3. Burlaga, L. F., Ness, N. F., & Richardson, J. D. 2003, Journal of Geophysical Research (Space Physics), 108, 8028
4. Cherny, G. G. 1988, Gas dynamics (M.: Nauka)
5. Coleman, Paul J., J. 1968, ApJ, 153, 371
6. Gamayunov, K., Zhang, M., Pogorelov, N., Heerikhuisen, J., & Rasoul, H. 2014, in Astronomical Society of the Pacific Conference Series, Vol. 484, Outstanding Problems in Heliophysics: From Coronal Heating to the Edge of the Heliosphere, ed. Q. Hu & G. P. Zank, 49
7. Gazis, P. R. 2000, J. Geophys. Res., 105, 19
8. Gazis, P. R., Barnes, A., Mihalov, J. D., & Lazarus, A. J. 1994, J. Geophys. Res., 99, 6561
9. Isenberg, P. A. 1986, J. Geophys. Res., 91, 9965
10. Isenberg, P. A., Smith, C. W., & Matthaeus, W. H. 2003, ApJ, 592, 564
11. Isenberg, P. A., Smith, C. W., Matthaeus, W. H., & Richardson, J. D. 2010, ApJ, 719, 716
12. Izmodenov, V. V. & Baranov, V. B. 2006, ISSI Scientific Reports Series, 5, 67
13. Lazarus, A. J., Belcher, J. W., Paularena, K. I., Richardson, J. D., & Steinberg, J. T. 1995, Advances in Space Research, 16, 77
14. Marsch, E. & Tu, C. Y. 1989, Journal of Plasma Physics, 41, 479
15. McNutt, R. L., Lyon, J., & Godrich, C. C. 1998, JGR, 103
16. Oughton, S., Matthaeus, W. H., Smith, C. W., Breech, B., & Isenberg, P. A. 2011, Journal of Geophysical Research (Space Physics), 116, A08105
17. Richardson, J. D., Liu, Y., Wang, C., & McComas, D. J. 2008, A&A, 491, 1
18. Richardson, J. D., Paularena, K. I., Lazarus, A. J., & Belcher, J. W. 1995, Geophys. Res. Lett., 22, 1469



19. Smith, C. W., Matthaeus, W. H., Zank, G. P., et al. 2001, J. Geo- phys. Res., 106, 8253
20. Usmanov, A. V., Goldstein, M. L., & Matthaeus, W. H. 2014, ApJ, 788, 43
21. Wang, C. & Richardson, J. D. 2001, J. Geophys. Res., 106, 29401 Wang, C. & Richardson, J. D. 2004, Journal of Geophysical Research (Space Physics), 109, A06104
22. Whang, Y. C. 1991, Space Sci. Rev., 57, 339
23. Williams, L. L., Zank, G. P., & Matthaeus, W. H. 1995, J. Geo- phys. Res., 100, 17059
24. Yermolaev, Y. I., Lodkina, I. G., Khokhlachev, A. A., et al. 2021, Journal of Geophysical Research (Space Physics), 126, e29618
25. Zank, G. P., Adhikari, L., Zhao, L. L., et al. 2018, ApJ, 869, 23 Zank, G. P., Hunana, P., Mostafavi, P., & Goldstein, M. L. 2014, ApJ, 797, 87
26. Zank, G. P., Matthaeus, W. H., & Smith, C. W. 1996, J. Geo- phys. Res., 101, 17093
27. Zhou, Y. & Matthaeus, W. H. 1990, J. Geophys. Res., 95, 14881
28. Carovillano, R. L.; and Siscoe, G. L.: Corotating Struc- ture in the Solar Wind. Solar Phys, Vol. 8, 1969, p. 401.
29. Chao, J. K. Interplanetary Collisionless Shock Waves. MIT center for Space Research preprint CSR TR-70-3, 1970.
30. Colburn, D. S.; and Sonett, C. P.: Discontinuities in the Solar Wind, Space Sci. Rev., Vol. 5, 1966, p. 439,
31. DeYoung, D. S.; and Hundhausen, A. J.: Non-spherical Propagation of a Flare- Associated Interplanetary Blast Wave (abstract), J. Geophys. Res., Vol. 76, 1971, p. 2245.
32. Dryer, M. and D. L. Jones: Energy Deposition in the Solar Wind by Flare-Generated Shock Waves. J. Geophys. Res., Vol. 73, 1968, p. 4875.
33. Gold, T. Gas Dynamics of Cosmic Clouds, edited by H. C. van de Hulst and J. M. Burgers, North-Holland Publishing Co., Amsterdam, 1955, p. 103.
34. Gosling, J. T; Asbridge, J. R.; Bame, S. J.; Hundhausen, A. J.; and Strong, I. B.: Measurements of the Inter- planetary Solar Wind During the Large Geomagnetic Storm of April 17-18, 1965. J. Geophys. Res., Vol. 72, 1967, p. 1813.
35. Hirshberg, J.: The Transport of Flare Plasma from the Sun to the Earth. Planet. Space Sci., Vol. 16, 1968, p. 309.



36. Hirshberg, J.; Alksne, A.; Colburn, D. S.; Bame, S. J.; and Hundhausen, A. J.: Observation of a Solar Flare Induced Interplanetary Shock and Helium-Enriched Driver Gas. *J. Geophys. Res.*, Vol. 75, 1970 p. 1.
37. Hundhausen, A. J.: Solar Wind Disturbances Associated with Solar Activity, in *Intercorrelated Satellite Observations Related to Solar Events*, edited by V. Manno and D. E. Page, D. Reidel, Bordrecht, 1970a.
38. Hundhausen, A. J.: Composition and Dynamics of the Solar Wind Plasma. *Rev. Geophys. Space Phys.*, Vol. 8, 1970b, p. 729.
39. Hundhausen, A. J.: Dynamics of the Outer Solar Atmosphere. Los Alamos Scientific Laboratory Preprint LA-DC-11911 (to be published in the proceedings of the Fourth Summer Institute for Astronomy and Astrophysics, Stony Brook) 1970c.
40. Hundhausen, A. J.: Shock Waves in the Solar Wind. *Particles and Fields in the Magnetosphere*, edited by B. M. McCormac, D. Reidel, Dordrecht, 79, 1970d.
41. Hundhausen, A. J.; and Gentry, R. A.: Numerical Simulation of Flare-Generated Disturbances in the Solar Wind. *J. Geophys. Res.*, Vol. 74, 1969a, p. 2908.
42. Hundhausen, A. J.; and Gentry, R. A.: The Effects of Solar Flare Duration on a Double Shock Pair at 1 AU. *J. Geophys. Res.*, Vol. 74, 1969b, p. 6229.
43. Lazarus, A. J.; and Binsack, J. H.: Observations of the Interplanetary Plasma Subsequent to the July 7, 1966 Proton Flare. *Ann. IQSY*, Vol. 3, 1969, p. 378.
44. Lazarus, A. J.; Ogilvie, K. W.; and Burlaga, L. F.: Interplanetary Shock Observations by Mariner 5 and Explorer 34. MIT Center for Space Research preprint CSR-P-70-\*36, submitted to *Solar Phys.*, 1970
45. Lee, T. S.; and Balwanz, W. W.: Singular Variations Near the Contact Discontinuity in the Theory of Interplanetary Blast Waves. *Solar Phys.* Vol. 4, 1968, p. 240.
46. Lepping, R. P.; and Argentiero, P. D.: Improved Shock Normals Obtained From Combined Magnetic and Plasma Data from a Single Spacecraft. NASA Goddard Space Flight Center Preprint X-692-70-276, 1970.
47. Mori, Y.: Shock Wave Hypothesis on Sudden Commencements of 27-Day Recurrent Geomagnetic Disturbances. *Sci. Rep. of Tohoku Univ.*, Series 5, Vol. 19, 1970, p. 135.
48. Petschek, H. E.: Reconnection and Annihilation of Magnetic Fields. *The Solar Wind*, edited by R. J. Mackin and M. Neugebauer, Pergamon Press, New York, 1966, p. 221.
49. Sturrock, P. A.: *Solar Flares. Plasma Astrophysics*, Academic Press, New York, 1967.



50. Taylor, H. E.: Sudden Commencement Associated Discontinuities in the Interplanetary Magnetic Field Observed by IMP 3. *SoZarPhys.*, Vol. 6, 1969, p. 320.
-

